JOURNAL OF APPLIED PHYSICS **124**, 173902 (2018)

Ground-state crystal structures of superconducting Nb_3Al and the phase transformation under high pressures

Jianjun Mao and Yue Chen[a)]
Department of Mechanical Engineering, The University of Hong Kong, Pokfulam Road, Hong Kong, China

(Received 29 August 2018; accepted 24 October 2018; published online 7 November 2018)

Niobium aluminide Nb_3Al, a typical A15 conventional superconductor, has been believed to adopt the cubic β-W type structure with a space group of $Pm\bar{3}n$ at ambient pressure since its discovery. Herein, we report a new crystal structure with a space group of C2/c, as predicted from the *ab initio* evolutionary algorithm, is energetically more favorable than the A15 phase at ambient pressure and low temperature. Phonon calculations indicate this phase is dynamically stable. The application of the Allen-Dynes modified McMillan equation to the C2/c phase yields a superconducting transition temperature T_c in the range of 17.44 – 19.48 K, which is in good agreement with experiments (18.8 K). A key difference between the A15 and C2/c crystal structures is the distortion of the Nb atomic chains, which are believed to be closely related to the superconducting behavior. Based on *ab initio* molecular dynamics simulations, we find that Nb_3Al transforms from the newly discovered C2/c phase to the standard A15 phase as temperature increases. Furthermore, another new phase with a space group of Cmcm is found to become stable as a hydrostatic pressure is applied. *Published by AIP Publishing.* https://doi.org/10.1063/1.5054071

INTRODUCTION

Over the last two decades, high cost and poor stabilization have inhibited large-scale applications of high-temperature cuprate superconductors,[1] and intermetallic niobium compounds remain the leading materials in superconducting applications. For example, the workforce of superconducting magnets is still Nb_3Sn,[2] although cuprate with higher T_c has been used for cell phone noise filters as superconducting high field (>30 T) magnets.[3] Compared with Nb_3Sn, Nb_3Al is more suitable for high-field applications because of its high critical field $H_{c2} = 29.5$ T at 4.2 K.[4] Moreover, it has also been shown that Nb_3Al becomes more robust under mechanical stress/strain conditions than the commercialized NbTi alloys and Nb_3Sn.[5] Therefore, Nb_3Al has been considered as an alternative to Nb_3Sn for high-energy particle accelerators, nuclear fusion, and gigahertz class nuclear magnetic resonance (NMR) analysis.

Viswanathan *et al.*[6] indirectly showed that the A15 phase of Nb_3Al is intrinsically unstable and undergoes a martensitic transformation at low temperatures from heat capacity measurements; however, the ground state crystal structure has yet to be determined. Recent experimental studies[7] revealed that martensitic transition plays an important role in the superconducting properties of the closely related V_3Si and Nb_3Sn A15 compounds. Through measurements of electrical resistance and specific heat, it was shown that the superconducting transition temperatures (T_c) of V_3Si and Nb_3Sn increase and gradually approach the martensitic transformation temperatures under high pressures, whereas further T_c enhancement is prohibited.

Crystal structure or atomic arrangement in a solid is critical for understanding the macroscopic properties of materials and the microscopic processes. Therefore, the determination of ground-state crystal structures of Nb_3Al is paramount. It is believed that Nb_3Al crystallizes in the A15 crystal structure with a space group of $Pm\bar{3}n$ at room temperature.[8,9] As can be seen from Fig. 1(b), the Y atoms in the X_3Y compound form a body-centered cubic (bcc) sublattice and each face is bisected by the non-intersecting orthogonal X (transition metal) atomic chains. The importance of these atomic chains is often emphasized on understanding the relatively high T_c of A15-type superconducting materials.

Measuring on polycrystalline Nb_3Al, Testardi *et al.*[10] observed a lattice softening via a decrease in the sound velocity at 300 K and 20 K by 2% and 4%, respectively. Using a high resolution electron microscope, Yoshida *et al.*[11] studied the microstructure of Nb_3Al at room temperature and 4 K. A contrast anomaly was observed at 4 K, which was believed to be related to the fluxoids in the superconducting state of Nb_3Al. In addition to the effects of temperature, Yu *et al.*[9] have reported that the volume of Nb_3Al showed an anomaly under high pressures. Furthermore, Smith[12] and Zhang *et al.*[13] found that the T_c of Nb_3Al decreases with increasing hydrostatic pressure. To better understand the above experimental observations, further theoretical studies on the ground state crystal structure and the pressure induced phase transitions are needed.

In this work, we conduct extensive crystal structure searches on Nb_3Al over a pressure range of 0 – 100 GPa, using the *ab initio* evolutionary algorithm. This method has recently been proven to be extremely powerful in discovering ground state crystal structures.[14–17] Our calculations reveal two new stable phases of Nb_3Al, of which the C2/c phase is believed to be directly related to the superconducting state at ambient pressure. Calculations of the phonon dispersions of

[a)]Author to whom correspondence should be addressed: yuechen@hku.hk

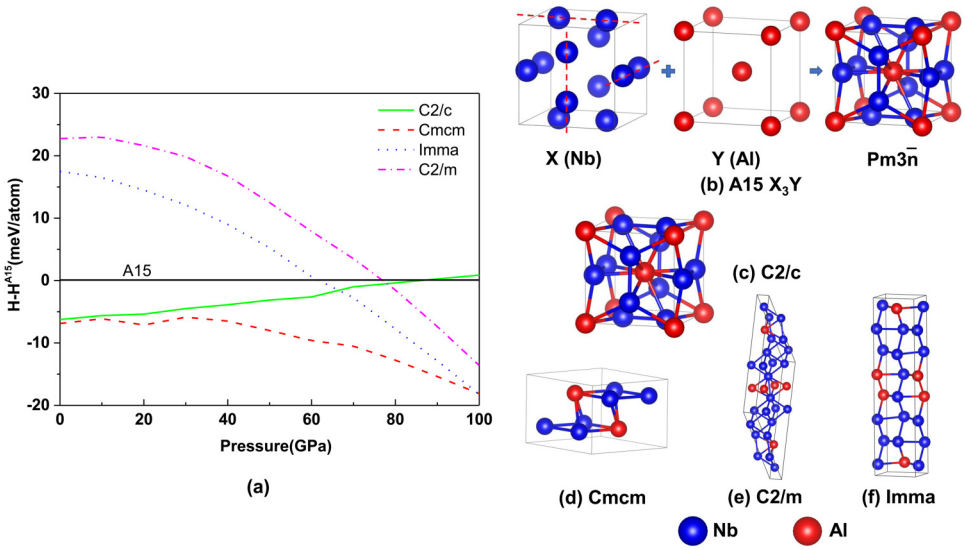

FIG. 1. (a) Enthalpies of competing crystal structures relative to the A15 phase of Nb_3Al in a pressure range of 0 – 100 GPa. (b) Known A15 cubic phase of Nb_3Al with a $Pm\bar{3}n$ symmetry; newly predicted phases of Nb_3Al with space groups of (c) C2/c, (d) Cmcm, (e) C2/m, and (f) Imma.

these new phases indicate that they are dynamically stable. Based on *ab initio* molecular dynamics (AIMD) simulations, we find that the C2/c phase of Nb_3Al transforms to the A15 phase at room temperature. From electron-phonon coupling (EPC) calculations, we obtain a theoretical T_c value of the C2/c phase, which is in good agreement with experiments. This work provides a more complete understanding of the ground state crystal structure of Nb_3Al and the pressure-induced phase transitions, which are closely related to the superconducting properties.

COMPUTATIONAL DETAILS

Ab initio evolutionary structure searches up to five formula units (f.u.) of Nb_3Al in the pressure range of 0 – 100 GPa in a 10 GPa interval were performed using USPEX.[18,19] The Vienna *Ab initio* Simulation Package (VASP)[20] within the framework of the density functional theory (DFT) was adopted to perform structural relaxations and electronic structure calculations. The Perdew-Burke-Ernzerhof[21] functional in the generalized gradient approximation (GGA)[22] was used. The electron-ion interactions were represented by the all-electron projector-augmented-wave method with $4p^6 4d^4 5s^1$ and $3s^2 3p^1$ treated as the valence electrons of Nb and Al, respectively. A plane-wave basis set cutoff of 500 eV and the Monkhorst-Pack (MP) scheme[23] with a dense k-point grid of $2\pi \times 0.03$ Å^{-1} spacing in the Brillouin zone (BZ) were adopted to ensure the enthalpy converges to 1 meV/atom. The convergence criterion of the electronic self-consistent iteration was set to 10^{-7} eV. Phonon calculations were performed using the supercell approach ($4 \times 4 \times 4$ supercell, 512 atoms)[24] as implemented in Phonopy.[25] *Ab initio* molecular dynamic simulations adopting the canonical (NVT) ensemble were performed with a time step of 1 fs for a total simulation time of ~5.2 ps at 10 K and 300 K. A supercell containing 216 atoms was used in the AIMD simulations and the system was initially equilibrated for 400 MD steps, and data were collected from the subsequent 4800 steps. The electron-phonon coupling (EPC) parameter was computed using density functional perturbation theory as implemented in Quantum ESPRESSO.[26] A kinetic energy cutoff of 80 Ry and norm-conserving pseudo-potentials were applied with $4 \times 4 \times 4$ and $4 \times 4 \times 6$ q-point meshes in the first Brillouin zones of the C2/c and Cmcm phases, respectively. For the EPC calculations, we used denser $16 \times 16 \times 16$ and $16 \times 16 \times 24$ MP k-meshes for the C2/c and Cmcm phases, respectively.

RESULTS AND DISCUSSIONS

Our evolutionary structure searches reveal two new phases of Nb_3Al with space group symmetries of C2/c and Cmcm. Both phases are found to be energetically more stable than the standard A15 phase at ambient pressure. Figure 1(a) shows the enthalpy-pressure relations for the different competing phases of Nb_3Al with respect to the known A15 ($Pm\bar{3}n$) phase. It is seen that as the pressure increases, the Cmcm phase becomes energetically more favorable. To examine the dynamical stabilities of the A15, C2/c, and Cmcm phases, we have calculated their phonon dispersions, as shown in Figs. 2 and 3. It is found that the A15 phase has large imaginary phonon frequencies near the Γ and X points, which indicate that the standard A15 phase is dynamically unstable at 0 K under ambient pressure. Meanwhile, the

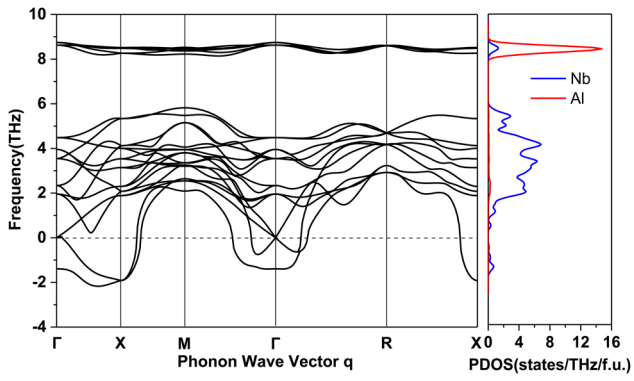

FIG. 2. Phonon dispersions of the A15 phase of Nb_3Al at ambient pressure (left). Negative values on the y axis denote imaginary phonon frequencies. Phonon DOS projected to the Nb and Al atoms (right).

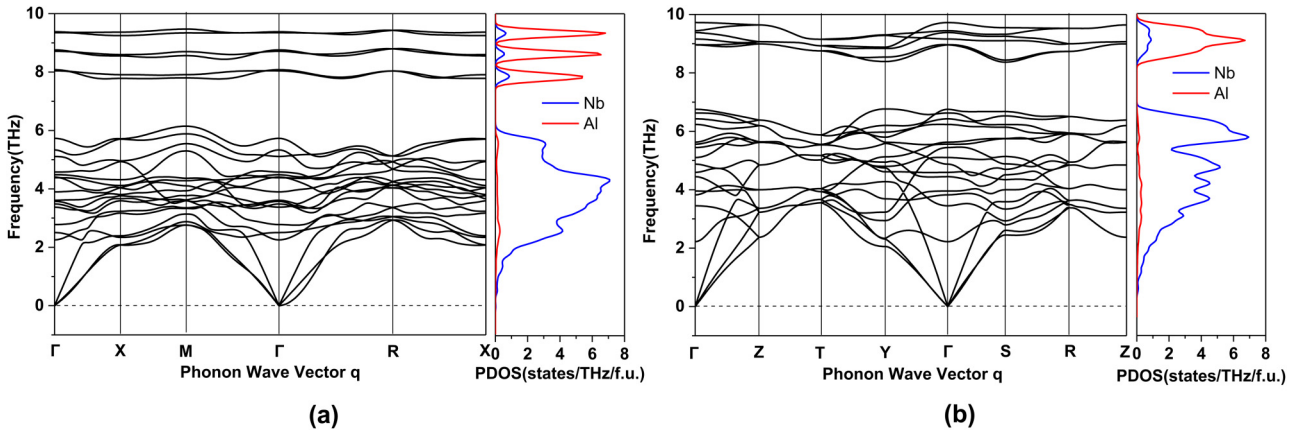

FIG. 3. Phonon dispersions and the projected DOS of the C2/c (a) and Cmcm (b) phases of Nb_3Al at ambient pressure.

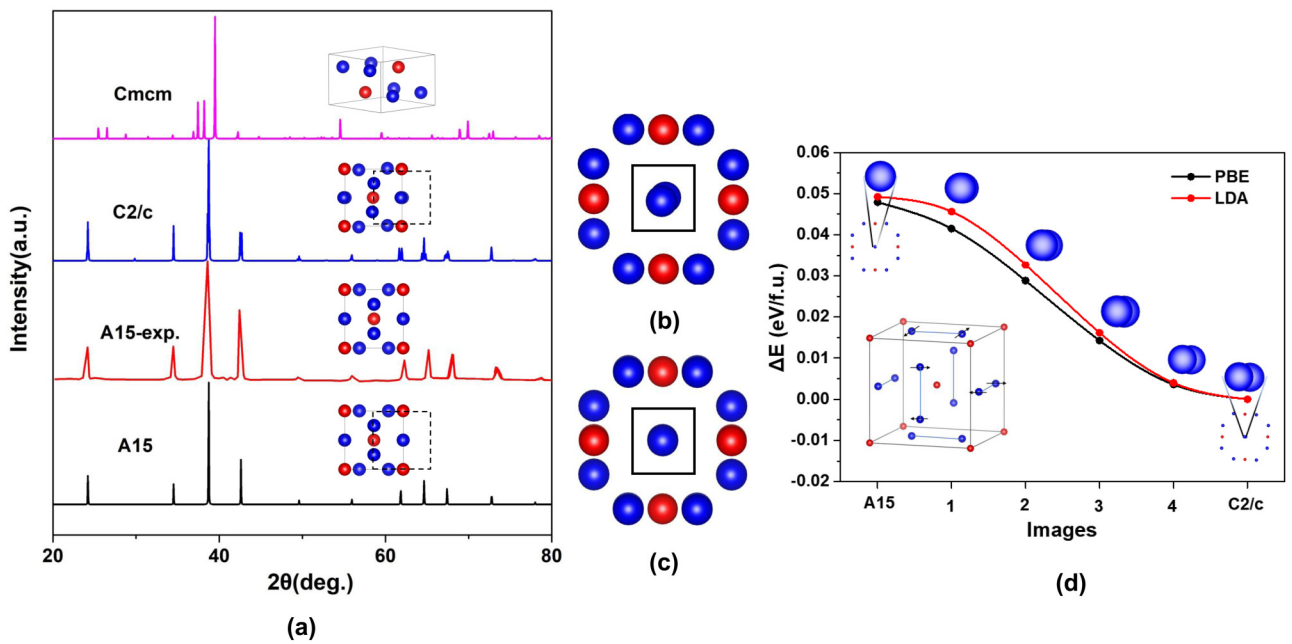

FIG. 4. (a) Simulated XRD patterns (λ = 1.54 Å) of the Cmcm, C2/c, and A15 phases along with the experimental XRD patterns of A15. Side views of the (b) C2/c and (c) A15 crystal structures. (d) Energy evolution accompanying the transformation from the A15 phase to the C2/c phase.

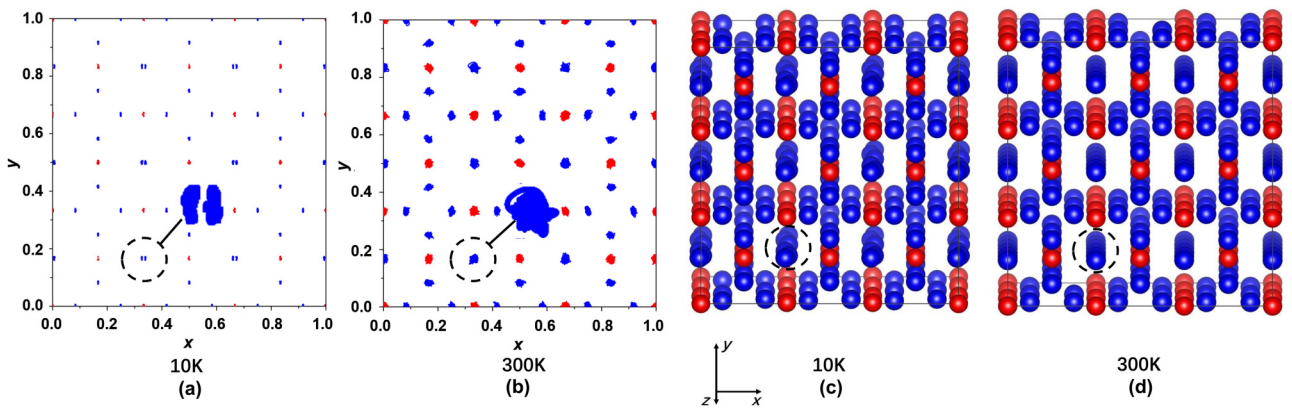

FIG. 5. Atomic trajectories of Nb (blue) and Al (red) projected onto the *xy* plane (a) and (b) and the average atomic positions (c) and (d) obtained from AIMD simulations. The A15 crystal structure has been taken to construct the initial supercell.

absence of imaginary frequencies in the first Brillion zone, as shown in Figs. 3(a) and 3(b), indicates that the C2/c and Cmcm phases are dynamically stable. From the site-projected phonon DOS, it is found that low-frequency modes are mainly associated with Nb atoms due to their larger atomic mass, whereas high-frequency modes are dominated by Al atoms. Compared with the Al high-frequency phonon bands in the A15 phase, the corresponding phonons in C2/c split into three different frequency domains. The vibrational modes of these optical branches at Γ point are shown in Fig. SI in the supplementary material for the A15 and C2/c phases. The high frequency vibrational modes of the Cmcm phase are shown in Fig. SII in the supplementary material. According to the enthalpy and phonon calculations, we show that Nb_3Al is likely to take the C2/c or the Cmcm crystal structure instead of the standard A15 structure at ambient pressure and very low temperatures. Detailed crystal structural information on the newly predicted C2/c and Cmcm phases is summarized in Table SI in the supplementary material.

The C2/c crystal structure is very similar to that of A15 with a subtle difference that can be observed from the side view as shown in Figs. 4(b) and 4(c). A key difference between the C2/c and A15 phases is the stacking of Nb atoms along the chain direction. To facilitate future experimental verification of the current theoretical results, we have simulated the XRD patterns of the C2/c, A15, and Cmcm phases, as shown in Fig. 4(a); the experimental XRD patterns of the A15 phase are also shown for comparison.[27] As expected, the simulated XRD patterns of A15 are in good agreement with the experimental results. The Nb sublattice distortion results in very small differences in the XRD patterns of the C2/c and the A15 phases; a similar phenomenon was also reported by Majumdar *et al.*[28] on AlI_3. Therefore, the so far undiscovered C2/c phase of Nb_3Al may be due to the difficulties in its observation from XRD experiments. On the other hand, the XRD patterns of the Cmcm phase are very different from those of the A15; thus, this phase should be easily observed if it exists. Considering the almost identical enthalpies of the C2/c and the Cmcm phases at ambient pressure as well as their distinct XRD patterns, the C2/c phase is more likely to exist; the following discussions on the superconducting transition temperatures also support the existence of the C2/c phase at ambient pressure. Nonetheless, the Cmcm phase may exist under high pressures as it gradually becomes energetically more favorable than the C2/c phase as pressure increases.

To provide further evidence on the stability of the C2/c phase at 0 K under ambient pressure, we have computed the energy evolution accompanying the transformation from A15 to C2/c. Four intermediate crystal structures in-between these two phases have been generated. It is seen from Fig. 4(d) that the total energy decreases monotonically as the A15 phase transforms to the C2/c phase, suggesting the robustness of our evolutionary crystal structure search.

To further investigate the temperature effects on the transformation between the A15 and C2/c phases, we have performed AIMD simulations using an A15 supercell under ambient pressure at 10 and 300 K. It is seen from Fig. 5 that a C2/c distortion exists at low temperature, which is consistent with the total energy calculations. Furthermore, a phase transition from C2/c to A15 is observed at 300 K. Although the exact phase transition temperature is not determined, our simulations provide an important insight into the low-temperature ground state crystal structure of Nb_3Al, which is directly related to its superconducting properties.

TABLE I. The logarithmic averages of phonon frequency (ω_{log}), electron-phonon coupling parameters (λ), and superconducting transition temperatures (T_c) of the C2/c and Cmcm phases at different pressures.

Phase	Pressure	λ	ω_{log} (K)	T_c (K, $\mu^*=0.1$)	T_c (K, $\mu^*=0.13$)
C2/c	0 GPa	1.28	202	19.48	17.44
Cmcm	0 GPa	0.44	201	1.50	0.82
	60 GPa	0.41	273	1.26	0.57
	100 GPa	0.41	295	1.41	0.64

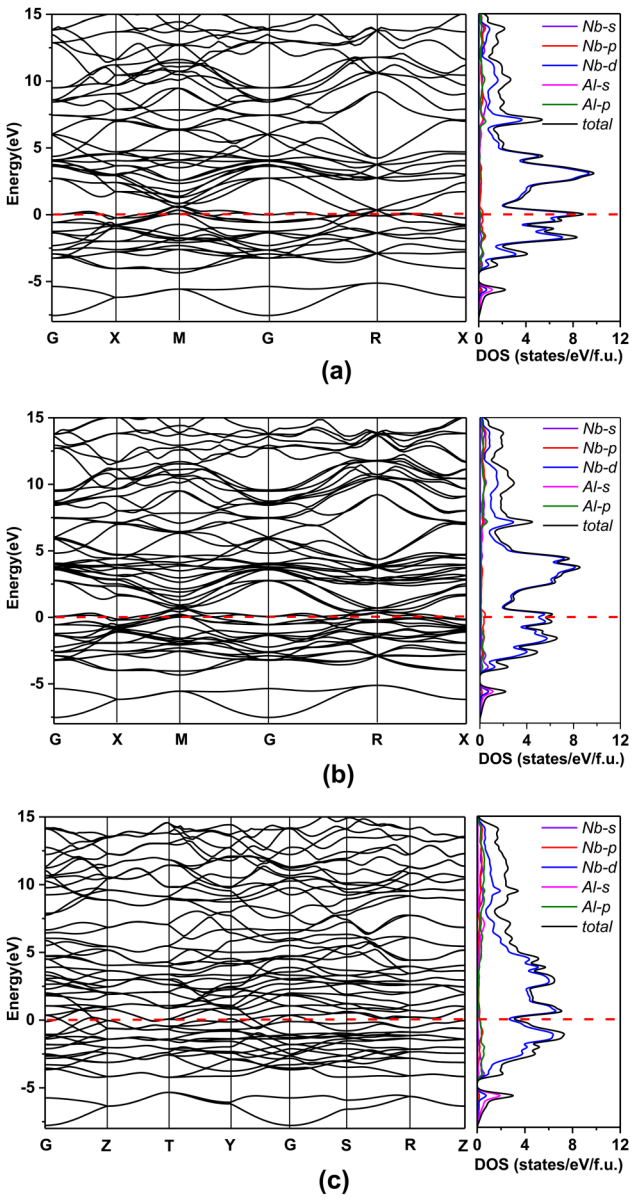

FIG. 6. Electronic band structures and projected density of states (DOS) of Nb_3Al in the (a) A15, (b) C2/c, and (c) Cmcm phases at ambient pressure. The Fermi level is located at 0 eV.

To explore the superconductivity of the newly predicted phases, we have further calculated their EPC parameter λ. The superconducting T_c can be estimated from the Allen-Dynes modified McMillan equation:[29]

$$T_C = \frac{\omega_{log}}{1.2} exp\left[\frac{-1.04(1+\lambda)}{\lambda - \mu^*(1+0.62\lambda)}\right], \quad (1)$$

where ω_{log} is the logarithmic average frequency and μ^* is the Coulomb pseudopotential. This equation has been found to be accurate for materials with $\lambda < 1.5$.[30] The logarithmic average frequency ω_{log} is calculated directly from the phonon spectrum, and μ^* is often taken as 0.1 – 0.13 for most metals. The EPC parameter λ is the reciprocal moment of the spectral function $\alpha^2F(\omega)$

$$\lambda = 2\int_0^\infty \frac{\alpha^2 F(\omega)}{\omega} d\omega \approx \sum_{qj} \lambda_{qj} w(\boldsymbol{q}), \quad (2)$$

and $w(\boldsymbol{q})$ is the weight of a $\boldsymbol{q}$ point (wave vector of crystal vibration) in the first BZ. The Eliashberg phonon spectral function $\alpha^2F(\omega)$ is expressed in terms of the phonon linewidths γ_{qj} arising from EPC[31]

$$\alpha^2F(\omega) = \frac{1}{2\pi N_f} \sum_{qj} \frac{\gamma_{qj}}{\omega_{qj}} \delta(\omega - \omega_{qj}) w(\boldsymbol{q}). \quad (3)$$

In the above equation, N_f represents the value of DOS at the Fermi level. The linewidth γ_{qj} and lifetime τ_{qj} of a phonon mode j at a wave vector $\boldsymbol{q}$, arising from EPC is given by

$$\gamma_{qj} = 2\pi\omega_{qj} \sum_{nm} \int \frac{d^3\mathbf{k}}{\Omega_{BZ}} |g^j_{kn,k+qm}|^2 \times \delta(\xi_{kn} - \xi_F) \times \delta(\xi_{k+qm} - \xi_F), \quad (4)$$

$$\tau_{qj} = \frac{1}{\gamma_{qj}}. \quad (5)$$

The sum is over the first BZ, of which the volume is Ω_{BZ}. ξ_{kn} denotes the Kohn-Sham[32] eigenvalue at wave vector $\boldsymbol{k}$ and ξ_F is the Fermi level. Here, $g^j{}_{kn,k+qm}$ is the electron-phonon matrix element for scattering an electron from band n at wave vector $\boldsymbol{k}$ to band m at wave vector $\boldsymbol{k}+\boldsymbol{q}$ via a phonon with a wave vector $\boldsymbol{q}$.

It is seen from Table I that the electron-phonon coupling parameter of the C2/c phase at 0 GPa is much larger than that of the Cmcm phase. As a result, the superconducting T_c of the C2/c phase is much higher; the theoretical T_c is in the range of 17.44 K – 19.48 K, which is in good agreement with the experimental superconducting transition temperature (18.8 K).[33] This further supports the existence of the predicted C2/c phase at ambient pressure. The Cmcm phase becomes more stable as the pressure increases; however, this phase has a rather low T_c due to the small λ value. This result invites us to probe the underlying superconducting mechanisms of these two phases.

In bcc Nb with a lattice parameter $a = 3.30$ Å, the shortest distance between two atoms is about 2.86 Å.[34] In the A15 phase of Nb_3Al with a lattice parameter of about 5.19 Å, the reduced Nb distance of 2.60 Å in the atomic chains is suggested to result in a large DOS near the Fermi level[35,36] as shown in Fig. 6(a). For a better understanding of the atomic chains in the A15 structure, we have calculated the electron localization function (ELF) and the charge density distribution as shown in Figs. SIV(a) and SIV(b) in the supplementary material. It is seen that the charge distribution along the Nb chains is the most prominent, and the ELF plot indicates dominant metallic bonding in Nb_3Al. For the C2/c phase shown in Fig. 6(b), a decrease of DOS at Fermi level is observed, which is dominated by the Nb-*d* states. A similar behavior was also observed in Nb_3Ge due to the dimerization of Nb atoms in the atomic chains, which induces a martensitic transformation.[37] The major difference is that Nb atoms move along the atomic chains in Nb_3Ge,[38] whereas they move perpendicular to the atomic chains in Nb_3Al. On the other hand, there is no Nb atomic chain in the Cmcm phase, of which the DOS at the Fermi level is also much lower [see Fig. 6(c)]. The decrease of DOS at the Fermi level is believed to be related to the lower superconducting T_c of the Cmcm phase. On the other hand, phonon lifetimes, Eliashberg phonon spectral function [$\alpha^2F(\omega)$], and

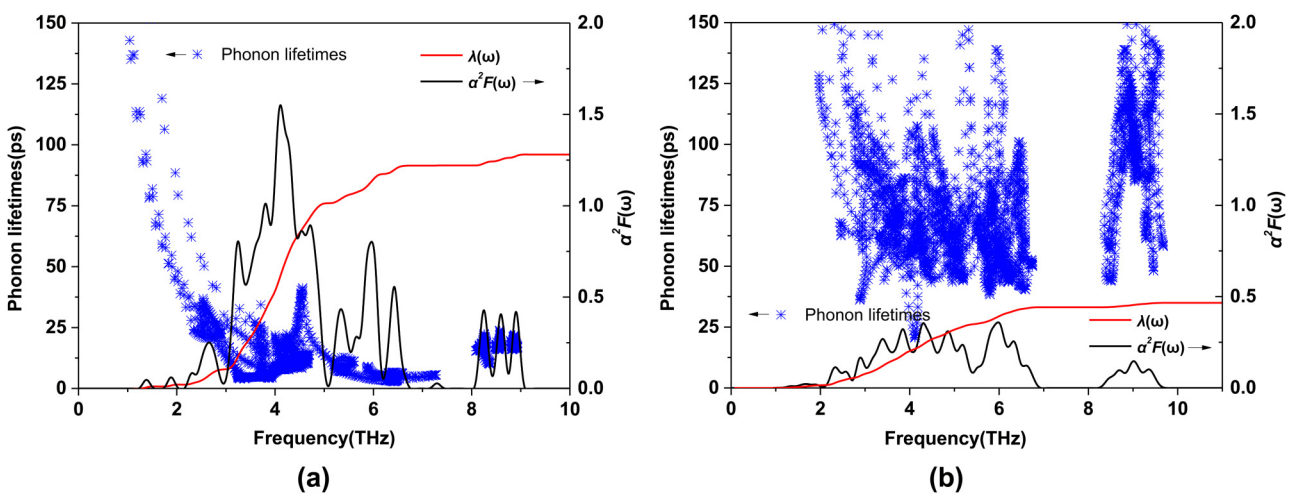

FIG. 7. Phonon lifetimes, Eliashberg phonon spectral function [$\alpha^2F(\omega)$], and electron-phonon integral [$\lambda(\omega)$] as a function of phonon vibration frequency of the (a) C2/c and (b) Cmcm phases.

electron-phonon integral [$\lambda(\omega)$] have also been calculated as shown in Fig. 7. It is found that the low-frequency vibration of the heavier Nb atoms contributes most to the total λ of both phases. The shorter phonon lifetimes of the C2/c phase indicate that the phonons, especially those mainly contributed by the Nb atoms, have stronger coupling with the electrons. Therefore, the higher T_c of the C2/c phase mainly originates from its distorted Nb atomic chains. The vibrational modes between 3 and 5 THz, which contribute most to the superconducting state, are shown in Fig. SV in the supplementary material.

CONCLUSION

Ab initio evolutionary structural searches have been performed for Nb_3Al over a pressure range of 0 – 100 GPa. Two new phases (C2/c and Cmcm) are discovered to be energetically more favorable than the standard A15 phase, and phonon calculations demonstrate that these new phases are dynamically stable. The C2/c and Cmcm phases have almost identical total energies at ambient pressure, while the C2/c phase is believed to be the major ground-state phase of Nb_3Al based on the simulated XRD patterns and the analysis on superconducting transitions. Nonetheless, the Cmcm phase becomes more energetically favorable as the pressure increases. It is also found from AIMD simulations that the newly discovered C2/c phase transforms to the A15 phase as temperature is increased. From electron-phonon coupling calculations, we obtain consistent superconducting transition temperature T_c of the C2/c phase with that observed in experiments. Our results provide important insight into the ground-state crystal structures and superconducting properties of Nb_3Al.

SUPPLEMENTARY MATERIAL

See supplementary material for vibrational modes of different Nb_3Al phases, simulated XRD patterns with Nb sublattices of Nb_3Al, charge density distribution in Nb_3Al, and crystallographic data of the competing phases of Nb_3Al at ambient pressure.

ACKNOWLEDGMENTS

This work is supported by the Research Grants Council of Hong Kong under Project Nos. 27202516, 17200017, and 17300018, and the National Natural Science Foundation of China under Project No. 51706192. The authors are grateful for the research computing facilities offered by ITS, HKU.

[1]A. Malozemoff, W. Carter, S. Fleshler, L. Fritzemeier, Q. Li, L. Masur, P. Miles, D. Parker, R. Parrella, and E. Podtburg, IEEE Trans. Appl. Supercond. **9**, 2469 (1999).
[2]I. Pong, S. Hopkins, X. Fu, B. Glowacki, J. Elliott, and A. Baldini, J. Mater. Sci. **43**, 3522 (2008).
[3]D. C. Larbalestier, J. Jiang, U. P. Trociewitz, F. Kametani, C. Scheuerlein, M. Dalban-Canassy, M. Matras, P. Chen, N. Craig, and P. Lee, Nat. Mater. **13**, 375 (2014).
[4]J. Muller, Rep. Prog. Phys. **43**, 641 (1980).
[5]W. Specking, H. Kiesel, H. Nakajima, T. Ando, H. Tsuji, Y. Yamada, and M. Nagata, IEEE Trans. Appl. Supercond. **3**, 1342 (1993).
[6]R. Viswanathan, C. Wu, H. Luo, and G. Webb, Solid State Commun. **14**, 1051 (1974).
[7]S. Tanaka, A. Miyake, T. Kagayama, K. Shimizu, P. Burger, F. Hardy, C. Meingast, and Y. Ōnuki, J. Phys. Soc. Jpn. **81**, SB026 (2012).
[8]Y. Chen, J. X. Shang, and Y. Zhang, J. Phys. Condens. Matter **19**, 016215 (2006).
[9]Z. Yu, C. Li, and H. Liu, Physica B **407**, 3635 (2012).
[10]L. Testardi, R. Soden, E. Greiner, J. Wernick, and V. Chirba, Phys. Rev. **154**, 399 (1967).
[11]H. Yoshida, H. Hashimoto, Y. Yokota, and M. Iwatsuki, Jpn. J. Appl. Phys. **26**, 943 (1987).
[12]T. Smith, J. Low Temp. Phys. **6**, 171 (1972).
[13]R. Zhang, P. Gao, X. Wang, and Y. Zhou, AIP Adv. **5**, 107233 (2015).
[14]Y. Chen, Q. M. Hu, and R. Yang, Phys. Rev. Lett. **109**, 157004 (2012).
[15]H. Yu and Y. Chen, J. Phys. Chem. C **122**, 15673 (2018).
[16]H. Yu, W. Lao, L. Wang, K. Li, and Y. Chen, Phys. Rev. Lett. **118**, 137002 (2017).
[17]W. Zhang, A. R. Oganov, A. F. Goncharov, Q. Zhu, S. E. Boulfelfel, A. O. Lyakhov, E. Stavrou, M. Somayazulu, V. B. Prakapenka, and Z. Konôpková, Science **342**, 1502 (2013).
[18]A. R. Oganov and C. W. Glass, J. Chem. Phys. **124**, 244704 (2006).
[19]A. R. Oganov, A. O. Lyakhov, and M. Valle, Acc. Chem. Res. **44**, 227 (2011).
[20]G. Kresse and J. Furthmüller, Phys. Rev. B **54**, 11169 (1996).
[21]J. P. Perdew, K. Burke, and M. Ernzerhof, Phys. Rev. Lett. **77**, 3865 (1996).
[22]J. P. Perdew, J. A. Chevary, S. H. Vosko, K. A. Jackson, M. R. Pederson, D. J. Singh, and C. Fiolhais, Phys. Rev. B **46**, 6671 (1992).
[23]H. J. Monkhorst and J. D. Pack, Phys. Rev. B **13**, 5188 (1976).
[24]K. Parlinski, Z. Li, and Y. Kawazoe, Phys. Rev. Lett. **78**, 4063 (1997).
[25]A. Togo, F. Oba, and I. Tanaka, Phys. Rev. B **78**, 134106 (2008).
[26]P. Giannozzi, S. Baroni, N. Bonini, M. Calandra, R. Car, C. Cavazzoni, D. Ceresoli, G. L. Chiarotti, M. Cococcioni, and I. Dabo, J. Phys. Condens. Matter **21**, 395502 (2009).
[27]X. Li, K. Ohsaki, Y. Morita, and M. Uda, J. Alloys Compd. **227**, 141 (1995).
[28]A. Majumdar, D. D. Klug, and Y. Yao, J. Chem. Phys. **144**, 124507 (2016).
[29]P. B. Allen and R. Dynes, Phys. Rev. B **12**, 905 (1975).
[30]C. Chen, Y. Xu, X. Sun, and S. Wang, J. Phys. Chem. C **119**, 17039 (2015).
[31]J. Dewhurst, S. Sharma, C. Ambrosch-Draxl, and B. Johansson, Phys. Rev. B **68**, 020504 (2003).
[32]W. Kohn and L. J. Sham, Phys. Rev. **140**, A1133 (1965).
[33]R. Willens, T. Geballe, A. Gossard, J. Maita, A. Menth, G. Hull, , Jr, and R. Soden, Solid State Commun. **7**, 837 (1969).
[34]M. Straumanis and S. Zyszczynski, J. Appl. Crystallogr. **3**, 1 (1970).
[35]A. Godeke, Supercond. Sci. Technol. **19**, R68 (2006).
[36]W. Weber, Phys. B **126**, 217 (1984).
[37]W. E. Pickett, K. Ho, and M. L. Cohen, Phys. Rev. B **19**, 1734 (1979).
[38]K. Ho, W. E. Pickett, and M. L. Cohen, Phys. Rev. B **19**, 1751 (1979).